Individual and Coupled Contributions of Laser Power and Scanning Speed towards Process-Induced Porosity in Selective Laser Melting

Subin Shrestha, Thomas Starr, Kevin Chou

Additive Manufacturing Research Center
University of Louisville
Louisville, KY 40292

Abstract

Porosity is an undesirable characteristic of selective laser melting (SLM) process and keyhole pores are formed when the energy density is very high which leads to deep penetration melting. In this study, single-track SLM experiments using Ti-6Al-4V powder were designed and conducted with combination of varied levels of the laser power and the scanning speed, intended to obtain the same energy density. Three energy densities: 0.32 J/mm, 0.4 J/mm and 0.48 J/mm were selected to investigate the influence of laser power versus scanning speed on porosity. Pore numbers and volumes was analyzed using micro-scale computed tomography. The results indicated that the pore formation is affected more by the change in the power than the scanning speed while keeping the energy density constant. As the power increased from around 20 W to 140 W, total pore volume increased, whereas pore volume decreased when power increased from 140 W to 195W.

Keywords: Computed tomography; Porosity; Selective laser melting.

1. Introduction

Selective laser melting (SLM) process has become a widely studied subject due to its freeform fabrication capability. However, inherent SLM defects such as porosity, part deformation are undesirable. Pores within the SLM fabricated samples have significant effect towards the part performance [1-3]. Leuders et al. demonstrated that the fatigue strength can be optimized by reducing the pore size as the stress concentration is reduced [4]. Besides the size of pore, its location is also critical to the stress concentration: pores near to surface were found more critical even if the size were smaller [5].

Pores, in general can be categorized as keyhole pores and metallurgical pores [6]. Keyhole pores are the result of keyhole mode melting which occurs when the energy density exceeds the keyhole threshold [7]. The energy density is the function of laser power, scanning speed, layer thickness and hatch spacing. Gong et al. [8] studied the effect of laser power and scan speed on the defect formation. Based on part quality, the power-speed curve can be divided into three zones: keyhole melting, conduction melting and incomplete melting. Pores can be formed when the energy density is very high or very low. Small amount of pores formed due to higher energy input are harmless when present up to 1 vol.% whereas defect due to insufficient energy input have effect even if the amount is as low as 1 vol.% [9]. Similarly, Aboulkhair et al. [6] investigated the effect of different process parameters to find the parameter window which

would produce high density parts from AlSi10Mg. The metallographic study showed that different pores such as keyhole pores and metallurgical pores may form depending upon the process parameters used. Besides, with AlSi10Mg, hydrogen porosity may form due to the presence of moisture in powder particle surface as well as dissolved hydrogen in the powder material. Ponnusamy et al. [10] performed statistical analysis on porosity of 17-4PH stainless steel. Effect of various process parameters such as laser power, defocus distance, layer thickness and build orientation were investigated which also helped to find optimum process parameters. Although, metallographic studies clearly reveal the pores present inside the sample, it does not provide complete information of pore distribution inside the whole sample.

As pore volume as well as pore location has significant effect on part performance, it is important to characterize pores formed due to different process conditions. Slotwinski et al. [11] performed porosity measurement on additively manufactured cobalt-chrome(Co-Cr) using X-Ray computed tomography (XRCT). XRCT technique help determine the morphology and distribution of pores within the sample. Siddique et al. [5] demonstrated that the percentage porosity calculated by two-dimensional metallography and three-dimensional tomography had no significant difference considering the critical pores. Kim et al. [12] utilized X-ray microtomography (μCT) to study the track changes in morphology of SLM Ti porous structures at different stage of post laser melting production. It has been demonstrated that μCT can be used not only for 3D quantification, but also as a feedback mechanism to make improvements on initial designs. Van Bael et al. [13] used XRCT as feedback mechanism to improve geometrical and mechanical controllability of selective laser melted Ti-6Al-4V porous structures. Ziolkowski et al. [14] explained the advantage of nondestructive XRCT over traditional metallograpic cross-sectional analysis. However, the major factor in XRCT is the resolution which would limit the pore size that can be studied.

In this study, the individual and coupled effect of power and scanning speed on single track porosity has been investigated. Different power and scan speeds were used to obtain three energy densities: 0.32 J/mm, 0.4 J/mm and 0.48 J/mm. Single tracks samples were fabricated and the internal pore feature were studied with micro-CT. Pore count and pore volume resulting from different process parameter have been compared.

2. Approach

SLM specimen fabrications

Hollow cylindrical samples have been designed as shown in Figure 1(a). The single tracks are formed on top of the solid semi-cylinder base. A constant spacing of 0.9 mm is maintained between single tracks and therefore each sample only contained four tracks. Two notches are used to identify the start and end of the single tracks. This design would also assist while performing CT scanning. Each sample has been marked as seen in Figure 1(a) to differentiate among the samples. In this study, three energy densities: 0.32 J/mm, 0.4 J/mm and 0.48 J/mm have been considered to study the effect of individual and coupled effect of power and scanning speed on porosity formation. The power and scanning speed used are presented in Table 1. The upper limit of power is maintained at maximum available laser power of 195 W. The design of experiment resulted in 12 tracks for 0.32 J/mm energy density while only 8 tracks are formed for

0.48 J/mm. Figure 1(b) shows the cylindrical samples with support on the build plate after fabrication. Three replicates have been produced for each sample.
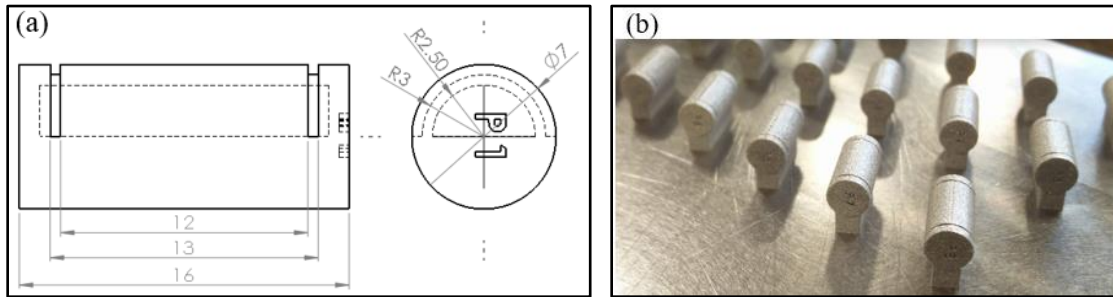

Figure 1: (a) CAD model of the specimen (unit in mm) and (b) Semi-hollow cylinders with single track built on the base plate.

Table 1: Process parameters used to form single tracks

ED(J/mm)	Speed(mm/s)	50	100	150	200	250	300	350	406.2	450	487.5	550	609.4
0.32		16	32	48	64	80	96	112	130	144	156	176	**195**
0.4	Power (W)	20	40	60	80	100	120	140	162.5	180	**195**	-	-
0.48		24	48	72	96	120	144	168	**195**	-	-	-	-

CT scanning

Bruker SkyScan 1173 micro-CT scanner as shown in Figure 2 is used to perform CT scanning of the fabricated samples. To align the sample with the X-ray source, brass sample mount with appropriate size is used. Clay, Styrofoam and parafilm tape were used to position sample on top of the brass sample mount as shown in Figure 2. Styrofoam and parafilm tape are preferred for the sample positioning as they are radiotransparent and do not affect the scanning of highly dense Ti-6Al-4V. Pixel resolution of 6 µm was used and samples were scanned at 2000 magnification. In order to transmit enough X-ray through highly dense titanium sample, high voltage of 130 kV x-ray source was generated which was filtered through a 0.25 mm brass filter so as to absorb x-ray with energy below 60 kV. This is necessary for highly dense materials to reduce beam hardening artifact otherwise the outer surface would appear more dense than interior due to higher absorbtion of low energy x-rays near outer surface. After obtaining raw images, steps towards reconstruction such as beam hardening correction, ring artifact reduction, misalignment compensation and smoothing were performed using parameter fine-tuning to minimize the ring artifacts and blurring effects, etc [15].

Figure 2: Specimen setup in the CT system (Left) and closed-up views (Right).

3. Results and Discussion

Typical scanning images

Figure 3 shows example of CT images from a typical specimen with different sectional views as well as the isometric partial cutoff view. The color coding is based on the density of the material: light grey area is solid, medium grey area is powder and the dark spots in the YZ cross section, which represent density of air, are pores. Four single tracks formed atop of base pad are clearly identified. These four tracks, in the figure shown are formed with laser power and scanning speed of 120W and 250 mm/s, 144 W and 300 mm/s, 168 W and 350 mm/s and 195W and 406.2 mm/s from left to right. The pores can be distinctly identified which are formed beneath the single track. These pores are mostly formed due to keyhole formation at high energy densities.
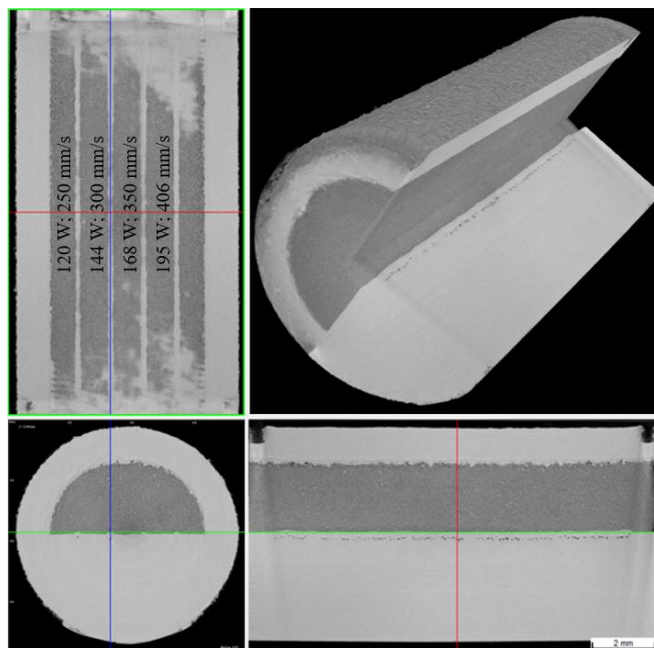

Figure 3: Examples of CT images of a scanned SLM specimen.

Single track morphology

CT scanning results were used to observe the track morphology as shown in Figure 4. It was noticed that at low power (24 W) and speed (50 mm/s), discontinuous track is observed even if high energy density is used. This may be due to lower power level: the input intensity is not enough to sufficiently melt the powder and substrate beneath to form a continuous melt pool. When both power and speed were doubled, a continuous track was observed. This track however had lower track width compared to other high power and speed cases. Figure 5 shows the average single track widths obtained with different scanning parameters. The track width for 24 W and 50 mm/s has not been considered due to discontinuous track. 48 W laser power with 100 mm/s speed only resulted in average track width of 146 μm, whereas track width beyond this power and speed were over 190 μm. For same energy density, lower power and lower speed resulted in track morphology as that of low energy density cases. But the melt pool width did not

increase with further increase in power and speed. This may be due to the keyhole mode melting: the flow is more dominant along the depth which resulted in almost similar melt pool width or track width.
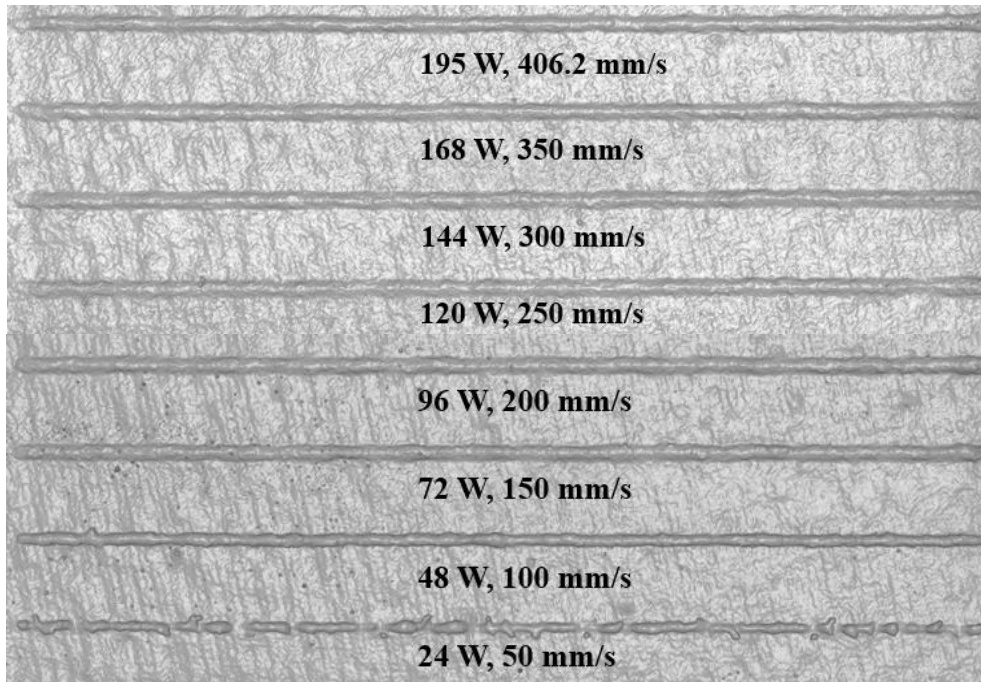

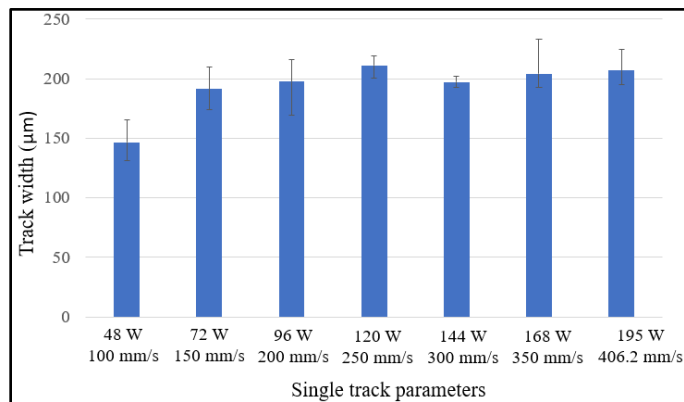Figure 4: Single track morphology at different process parameters for ED=0.48 J/mm.

Figure 5: Track width from different scanning parameters for ED=0.8 J/mm.

Process effect

The transverse sections of single tracks have been presented in Figure 6. The transverse section of single track with 24 W, 50 mm/s shows wavy profile due to discontinuity in the track. As the power and speed were increased, the waviness was reduced and continuous, dense tracks were formed. Single tracks with 48 W and 72 W did not reveal pores, while as the power increased beyond 72 W, numerous pores were observed. This means that even for same energy density, keyhole mode melting highly depend on the level of power used. These pores are analyzed to compare the pore count and the pore volume among the fabricated single tracks.
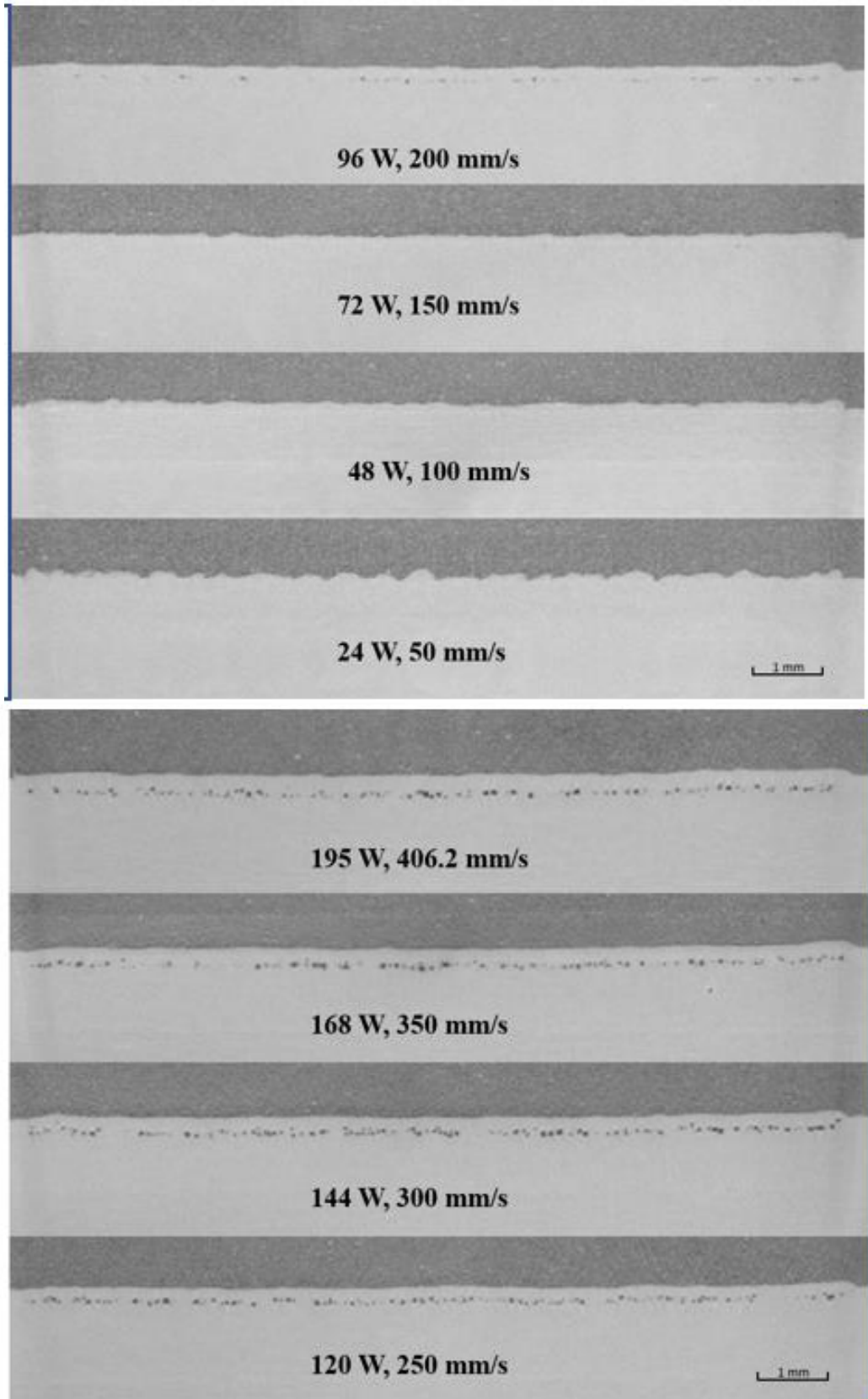
Figure 6: Transvere sections from single track with ED=0.48 J/mm.

The pore analysis is performed over reconstructed image to obtain quantitative pore information. The raw images are transformed into binary images to calculate pore volume, surface area, sphericity etc. Then, 3D rendered pores are also generated. Figure 7 explains how the binary images of a pore at successive slices are used to obtain the rendered 3D representation of a pore.
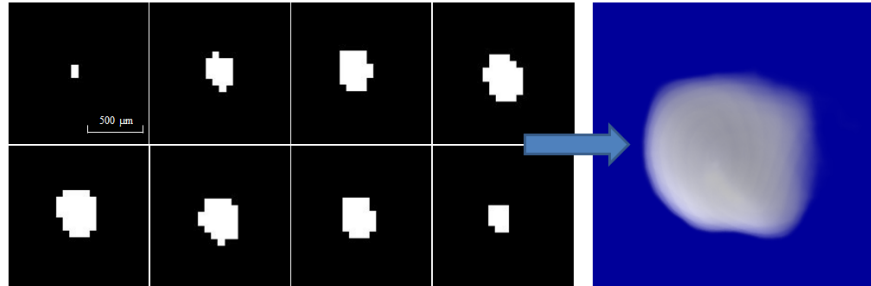

Figure 7: 3D rendering of a pore from 2D binary images [15].

The effect of power and scan speed on pore count and pore volume have been summarized in Figure 8. As the power and speed increased for same energy density, the pore count and the total pore volume increased. At low power and low speed, no or very few pores were observed. The pore count increased singnificantly around power 100 W and continued to increase until 140 W. In all three energy density cases, maximum volume of pores was observed when Power was around 140 W although scan speed were different: 144 W and 450 mm/s for 0.32 J/mm energy density, 140 W and 350 mm/s for 0.4 J/mm energy density and 144 W and 300 mm/s for 0.48 J/mm energy density. As the power and speed increased beyond this point, there is a significant drop in pore count and volume.
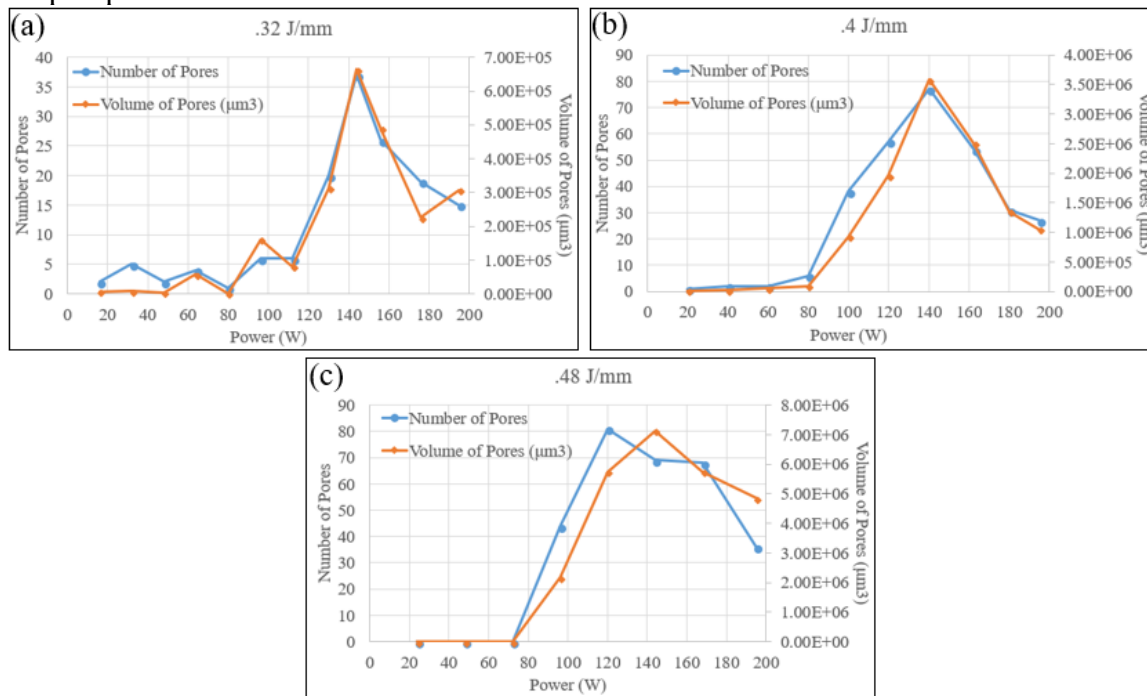

Figure 8: Pore count and pore volume obtained at different process parameters from different energy densities (a) 0.32 J/mm, (b) 0.4 J/mm and (c) 0.48 J/mm.

The penetration depth of keyhole is directly proportional to laser power and inversely proportional to the scan speed [16]. Also, power has more effect towards the maximum temperature in melt pool compared to scanning speed [7]. When we assume that melt pool depth normalized by the beam radius is only a function of ratio of deposited energy density to the enthalpy at melting:

$$\frac{\Delta H}{h_s} = \frac{AP}{\pi h_s \sqrt{D u \sigma^3}}$$ (1)

Where, ΔH is specific enthalpy, h_s is enthalpy at melting, A is absorptivity, P is power, D is thermal diffusivity of the molten material, u is beam travel speed and σ is beam size.

From equation 1, we may say that pore count and volume would increase with increasing power due to increase in keyhole effect. However this was not always true for the same energy density as increasing power after certain level decreased. It was interesting to see the similar trend in pore volume curve, with higher energy densities resulting in higher pore volume. We may also say that power is more significant towards the pore volume as the critical power seems to be similar for all three cases. The relation $P/\sqrt{u}$ is used to reduce the effect of speed on the graph which is shown in Figure 9. If magnitude of speed is further decreased, then the critical point would be aligned in a straight vertical line.

From the track morphology and porosity results, we observe that from the experimental settings used, the critical power is around 140 W. When the power and speed is decreased from 140 W, the track width decreased along with the porosity. And when the power and speed increased, the track width remained almost constant while reduction in pore number and the pore volume. It would be interesting to see what would be the porosity level beyond power level of 195 W for same energy density.
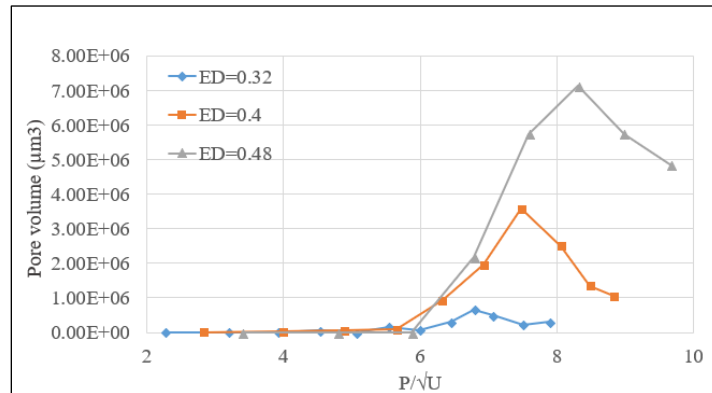

Figure 9: Coupled effect of power and speed on pore volume

The pores are formed at different depth with different process parameters. It is difficult to explain the penetration depth resulted from different power level with the study of porosity alone. However, we can make a statement that pore depth would provide initial idea on how deep the keyhole penetration is. The keyhole penetration seemed to increase with increasing power and speed. A metallographic study is required to have better understanding of this phenomenon.

4. Conclusions

Porosity analysis in SLM single-track specimens was performed using a SkyScan 1173 micro-CT scanner. The results clearly show pores resulted from the keyhole phenomenon and following conclusions can be made from this study:

- The keyhole behavior is more affected by power than scan speed. As the power increases for same energy density, pore volume increased even if scanning speed increased.
- At same energy density, the lower power would result in balling behavior which is observed at low energy density melting: the input intensity may not be enough to properly melt the powder and substrate.
- Pore volume is maximum at around 140 W laser power. As the power further increased pore number and pore volume decreased for the interval of power investigated in this paper.

The maximum power studied is limited to 195 W due to the limitation of EOS M270 power output. It would be interesting to see if the pore number and volume would further decrease with increasing power and scanning speed for studied energy densities.

References

[1] Cherry, J., Davies, H., Mehmood, S., Lavery, N., Brown, S., and Sienz, J., 2015, "Investigation into the effect of process parameters on microstructural and physical properties of 316L stainless steel parts by selective laser melting," The International Journal of Advanced Manufacturing Technology, 76(5-8), pp. 869-879.

[2] Edwards, P., and Ramulu, M., 2014, "Fatigue performance evaluation of selective laser melted Ti–6Al–4V," Materials Science and Engineering: A, 598, pp. 327-337.

[3] Siddique, S., Imran, M., Wycisk, E., Emmelmann, C., and Walther, F., 2015, "Influence of process-induced microstructure and imperfections on mechanical properties of AlSi12 processed by selective laser melting," Journal of Materials Processing Technology, 221, pp. 205-213.

[4] Leuders, S., Thöne, M., Riemer, A., Niendorf, T., Tröster, T., Richard, H., and Maier, H., 2013, "On the mechanical behaviour of titanium alloy TiAl6V4 manufactured by selective laser melting: Fatigue resistance and crack growth performance," International Journal of Fatigue, 48, pp. 300-307.

[5] Siddique, S., Imran, M., Rauer, M., Kaloudis, M., Wycisk, E., Emmelmann, C., and Walther, F., 2015, "Computed tomography for characterization of fatigue performance of selective laser melted parts," Materials & Design, 83, pp. 661-669.

[6] Aboulkhair, N. T., Everitt, N. M., Ashcroft, I., and Tuck, C., 2014, "Reducing porosity in AlSi10Mg parts processed by selective laser melting," Additive Manufacturing, 1, pp. 77-86.

[7] King, W. E., Barth, H. D., Castillo, V. M., Gallegos, G. F., Gibbs, J. W., Hahn, D. E., Kamath, C., and Rubenchik, A. M., 2014, "Observation of keyhole-mode laser melting in laser powder-bed fusion additive manufacturing," Journal of Materials Processing Technology, 214(12), pp. 2915-2925.

[8] Gong, H., Rafi, K., Gu, H., Starr, T., and Stucker, B., 2014, "Analysis of defect generation in Ti–6Al–4V parts made using powder bed fusion additive manufacturing processes," Additive Manufacturing, 1, pp. 87-98.

[9] Gong, H., Rafi, K., Gu, H., Ram, G. J., Starr, T., and Stucker, B., 2015, "Influence of defects on mechanical properties of Ti–6Al–4 V components produced by selective laser melting and electron beam melting," Materials & Design, 86, pp. 545-554.

[10] Ponnusamy, P., Masood, S., Ruan, D., Palanisamy, S., and Mohamed, O., "Statistical analysis of porosity of 17-4PH alloy processed by selective laser melting," Proc. IOP Conference Series: Materials Science and Engineering, IOP Publishing, p. 012001.

[11] Slotwinski, J. A., Garboczi, E. J., and Hebenstreit, K. M., 2014, "Porosity measurements and analysis for metal additive manufacturing process control," Journal of research of the National Institute of Standards and Technology, 119, p. 494.

[12] Kim, T. B., Yue, S., Zhang, Z., Jones, E., Jones, J. R., and Lee, P. D., 2014, "Additive manufactured porous titanium structures: Through-process quantification of pore and strut networks," Journal of Materials Processing Technology, 214(11), pp. 2706-2715.

[13] Van Bael, S., Kerckhofs, G., Moesen, M., Pyka, G., Schrooten, J., and Kruth, J.-P., 2011, "Micro-CT-based improvement of geometrical and mechanical controllability of selective laser melted Ti6Al4V porous structures," Materials Science and Engineering: A, 528(24), pp. 7423-7431.

[14] Ziółkowski, G., Chlebus, E., Szymczyk, P., and Kurzac, J., 2014, "Application of X-ray CT method for discontinuity and porosity detection in 316L stainless steel parts produced with SLM technology," Archives of Civil and Mechanical Engineering, 14(4), pp. 608-614.

[15] Shrestha, S., Shrestha, S., and Chou, K., "Porosity Analysis in Metal Additive Manufacturing by Micro-CT," Proc. ASME IMECE Conference(accepted).

[16] Fabbro, R., 2010, "Melt pool and keyhole behaviour analysis for deep penetration laser welding," Journal of Physics D: Applied Physics, 43(44), p. 445501.